CHAPTER

# THE ROMPAS PROSPECT, PERÄPOHJA SCHIST BELT, NORTHERN FINLAND

# 5.4

**E. Vanhanen, N.D.J. Cook, M.R. Hudson, L. Dahlenborg, J.-P. Ranta, T. Havela, J. Kinnunen, F. Molnár, A.R. Prave, N.H.S. Oliver**

## ABSTRACT

The Rompas prospect in the Ylitornio municipality is one of the most exciting recent discoveries in Finland. Spectacular bonanza grades, with abundant visible gold in association with uraninite, are hosted within deformed dolomite–calc-silicate–quartz veins in metabasalts along a 6-km-long ridgeline. The highest gold grades are associated with texturally late, sulfur-bearing pyrobitumen inferred to have formed at least 150° cooler than peak metamorphic conditions, approximately 150 million years after the crystallization of the vein-hosted uraninite.

**Keywords:** Finland; Peräpohja; Rompas; gold; uranium; uraninite; pyrobitumen; dolomite; calc-silicate; Svecofennian orogeny.

## INTRODUCTION

The Rompas gold-uranium prospect is located in Ylitornio municipality, northern Finland, at 66.45 °N and 24.75 °E. It lies some 50 kilometers (km) to the west of Rovaniemi, the administrative capital of Lapland. Rompas was discovered by AREVA Resources Finland Oy in September 2008 as part of regional uranium exploration (Fig. 5.4.1). Limited exploration was undertaken until Mawson Resources purchased the exploration assets of AREVA in 2010 and subsequently defined more than 300 surficial bonanza-grade Au grab and channel samples from vein style mineralization over a north-trending strike of 6 km within the Peräpohja schist belt. Diamond drilling in 2012 and 2013 produced numerous Au-U rich intersections, of which 6 m at 617 g/t Au remains the highlight (in drill hole ROM0011). High fineness native gold and uraninite are the key economic minerals discovered to date.

The Peräpohja schist belt is not yet recognized as a mineral belt of high potential. The only active mine is the Kemi chromium mine, and that is within basal-layered mafic and ultramafic rocks (Halkoaho and Iljina, 2012). Kyläkoski et al. (2012a) describe quartz-carbonate vein-hosted and dolerite-hosted Cu-Au occurrences in addition to the Vähäjoki deposit ascribed to the iron oxide-copper-gold (IOCG) grouping (see also Eilu et al., 2007). In the northeastern Peräpohja schist belt, small tremolite and serpentine skarn magnetite occurrences are potentially of the IOCG class (Niiranen et al., 2003; Niiranen, 2012, and references therein). Details of the Rompas prospect to date have been largely restricted to internal Mawson Resources reporting and press releases available on the Mawson Resources website. Since discovery of the Rompas prospect, the Palokas prospect has been discovered approximately 8 km to the east. Gold

**Mineral Deposits of Finland.** http://dx.doi.org/10.1016/B978-0-12-410438-9.00018-2

mineralization at Palokas is a different style from Rompas, with gold and bismuth tellurides associated with pyrrhotite, ilmenite, magnetite, and scheelite within a variety of magnesian silicate minerals.

Mawson holds 833 claims and claim applications for 75,340 hectares at the Rompas Project. A total of 110 exploration claims that cover a surface area of 10,580 ha and form the core claims at Rompas came into legal force on October 15, 2012. The Natura 2000 network (European-defined biodiversity areas) is extensive in north Finland and has limited drill access to targets below the strongest Au and U anomalies. More than 90% of the strike extent of the Rompas prospect lies within the Natura 2000 designated areas. Applications have been made to the relevant Finnish granting authorities to allow diamond-drill testing of targets. Thus the drill results used here are from 84 diamond drill holes of less than 200 m down-hole depth, with the majority less than 110 m. The drill areas form only a very small portion of the prospect area (estimated at less than 5%). We expect that the understanding of the prospect will change significantly following better drill access in the coming years.

The descriptions and interpretations in this chapter are largely confined to field and drill core observations combined with geochemical and petrographic descriptions to confirm the nature of the major rock types. Detailed petrologic and isotopic work in progress by Ferenc Molnár and coworkers at GTK (Geological Survey of Finland) and Harry Oduro of the University of St Andrews (Scotland) is fast advancing the knowledge of the relationship of uraninite and gold at Rompas.

## REGIONAL GEOLOGY

The Rompas prospect lies within the Peräpohja schist belt (PSB), a Paleoproterozoic supracrustal sequence of quartzites, mafic volcanics and volcaniclastics, carbonate rocks, black shales, mica schists, and graywackes that unconformably overlies Archean rocks of the Pudasjärvi complex (Fig. 5.4.1). Deposition of volcanics and sediments of the Peräpohja commenced after 2.44 Ga (Huhma et al., 1990) with the youngest rocks deposited after approximately 1.91 Ga based on inherited zircon populations in the Martimo formation (Ranta, 2012; Ranta et al., in prep.). We believe it is likely that the bulk of the mapped lowermost PSB was deposited on a relatively low gradient surface, either emergent (regionally extensive quartz sandstones) or shallow water (stromatolitic carbonate rocks). Also within the sequence are inferred evaporites of the Petäjäskoski formation (Kyläkoski et al., 2012b). Toward the end of the history of the PSB, however, traction current related sediments, reflecting basinal development, dominated the sequence (Korkiavaara, Pöyliövaara, and Martimo formations). The nature of the depositional environment and the interpreted long history of the PSB makes the likelihood of regional unconformities very high.

Correlation of rocks of the PSB sequence with the apparently similar Russian stratigraphy described in the Far Deep Project volumes (Melezhik et al., 2013) has been made by Prave (2013, internal company reporting) who proposed three major basin stages (Fig. 5.4.2). First, a continental margin dominated by nonmarine siliciclastic rocks and mafic volcanism with potentially two glacial episodes included: the Sompujärvi and the younger Kaisavaara glacials. The second basinal stage involves a change to shallow to nonmarine deposition of carbonate rocks and quartzites and is recognized as including the Lomagundi-Jatuli episode of enhanced $\delta^{13}C$ deposition (Karhu, 1993; Huhma et al., 2011). The third depositional stage involves development of considerable topographic relief. Basinal deepening with arkosic and quartzose turbidite fans are synchronous with mafic and felsic volcanism (e.g., Hanski et al., 2005). We propose that strike-slip tectonics are driving both transpressional and transtensional stress regimes resulting in both the uplift and the basin formation during this third depositional stage. This is likely synchronous with metamorphism and the emplacement of igneous intrusives.

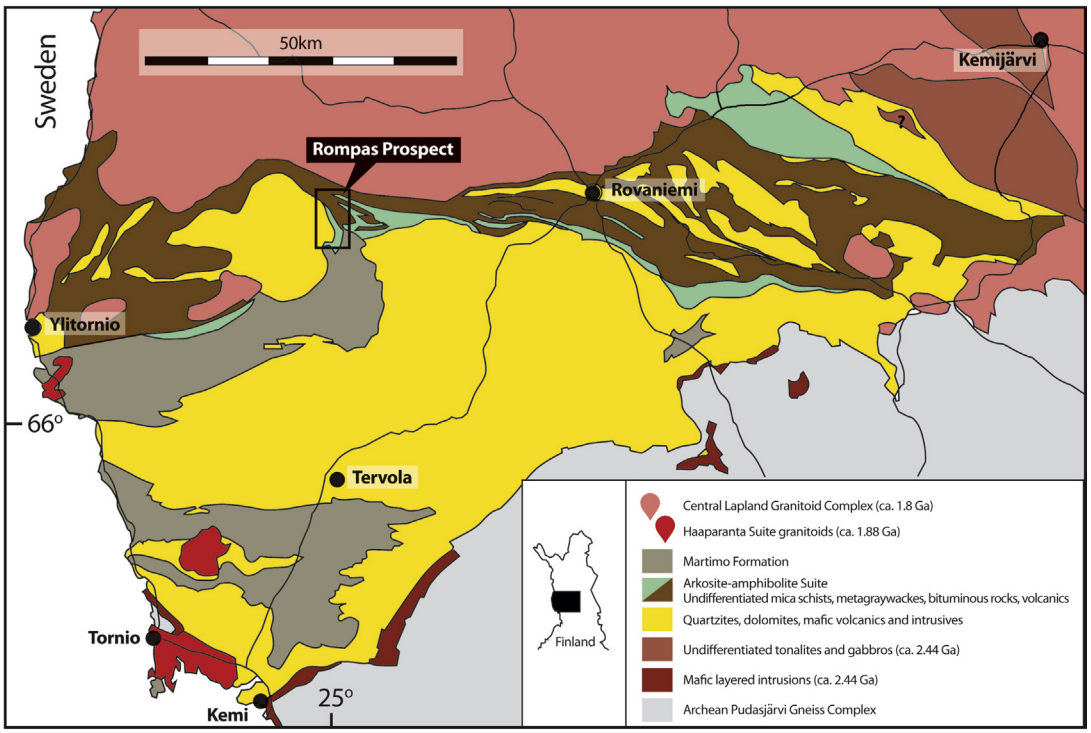


**FIGURE 5.4.1 Regional geology and location details of Rompas prospect, Ylitornio, northern Finland.**

This map is modified largely from Hanski et al. (2005) by grouping the arkosic-amphibolite suite with the formations inferred to be below the Martimo formation, but within the "late basin stages" as detailed in the text and Fig. 5.4.2. Lauri (personal communication, 2013) has also indicated the presence of approximately 2.44 Ga tonalities and gabbros in the Kemijärvi area (northeast corner of the map).

Metamorphism ranges from mid or upper greenschist facies in the south of the PSB to amphibolite facies conditions in the northern part of the belt, where Rompas is also located. To the north of Rompas, the pelitic compositions contain abundant migmatites and are intruded by granitoids of the Central Lapland Granite Complex (e.g., Perttunen et al., 1996; Lauri, 2012). The Sm-Nd data on tourmaline granites intruding the migmatites give ages of approximately 1.78 Ga (Ranta, 2012).

Deformation in the Peräpohja schist belt varies in style, largely related to the metamorphic grade. In the southern, greenschist facies portions, open to tight folds dominate, with a strong indication of thrust-related folding where axial surfaces are commonly broken by small thrust faults. As metamorphic grade increases to the north toward the Central Lapland Granite Complex, the fold intensity and strain increase dramatically and is typified by isoclinal to tight folds, with the highest strain occurring in the upper parts of the sequence that is dominated by thinly bedded sediments, mafic, and carbonate rocks. This may reflect the reactivation of basin-controlling structures. We believe that in the Rompas area, the rocks of the uppermost second basinal and third basinal stages (Fig. 5.4.2) have taken much of the shortening strain during the amphibolite facies metamorphism. Repeated thrust faulting and folding is evident west of Rompas where repetition of thin conductive graphitic rocks marks repeats of the stratigraphic sequence.

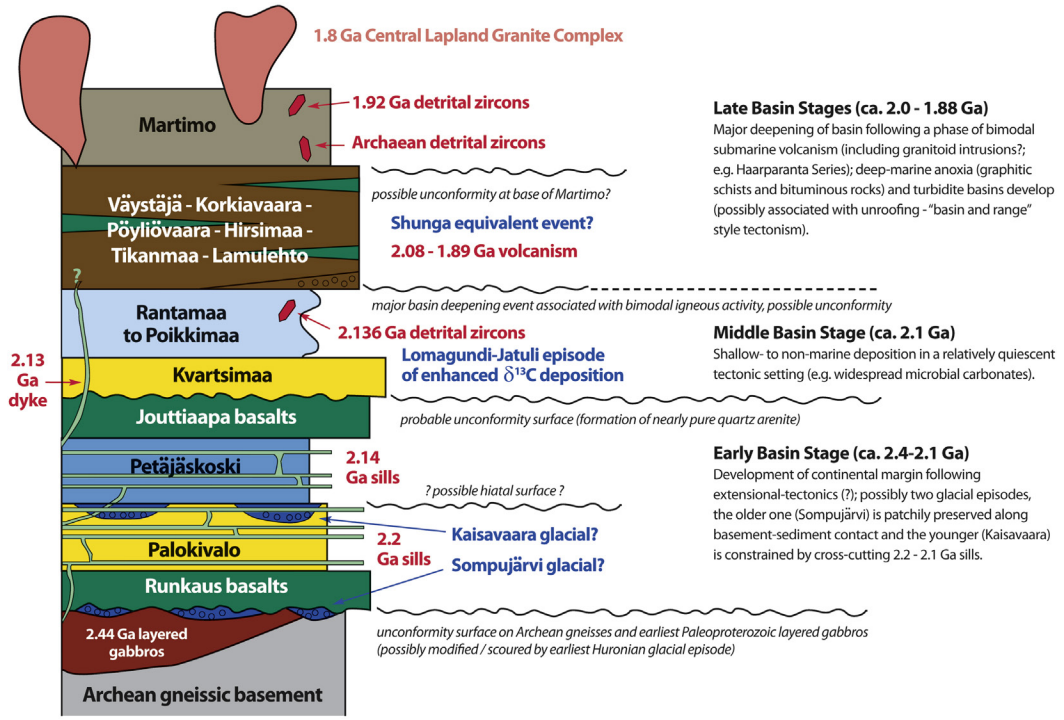


**FIGURE 5.4.2 Proposed stratigraphic subdivision of the Peräpohja schist belt.**

We interpret the Rompas prospect to lie in rocks deposited near the top of the middle basin stage, within the platform carbonate and quartzite rocks above the Jouttiaapa basalts, and in close contact with the overlying late basin stage rocks (metamorphosed turbiditic clastic sediments, carbonates, carbon-rich sediments, and mafic rocks). The stratigraphic column shows formation names for the PSB, largely based on Perttunen and Hanski (2003) and Kyläkoski et al. (2012b).

## ROMPAS AREA GEOLOGY

The Rompas prospect area (Fig. 5.4.1) is dominated by a north-trending resistant ridge formed by metabasalt, carbonate-rich, and carbonate-albite rocks (Fig. 5.4.3). On the ridge crest, these rocks either crop out or are covered by a thin glacial till (generally less than 1 m). On either side of the ridge, small lakes, peat bogs, and thicker till are abundant with isolated bedrock outcrops. However, Au-U mineralized rock in the metabasalts is known to continue under deeper till cover on both sides of the ridge (Fig. 5.4.4). The metabasalts are generally fine to medium grained, dominated by the assemblage of plagioclase, quartz, amphibole, and biotite. Original igneous textures are absent from South Rompas (e.g., Fig. 5.4.5), and variably preserved at North Rompas (Fig. 5.4.6). At North Rompas, we interpret some textures to represent interflow sediment remnants and deformed amygdales, now rich in biotite.

The albitic calc-silicate-bearing rocks that lie between the mafic units are generally paler, owing to more abundant albite and quartz and lesser biotite and amphibole. Where highly foliated and veined with calc-silicate-carbonate-quartz, the metabasalts can be hard to distinguish from the metasediments.

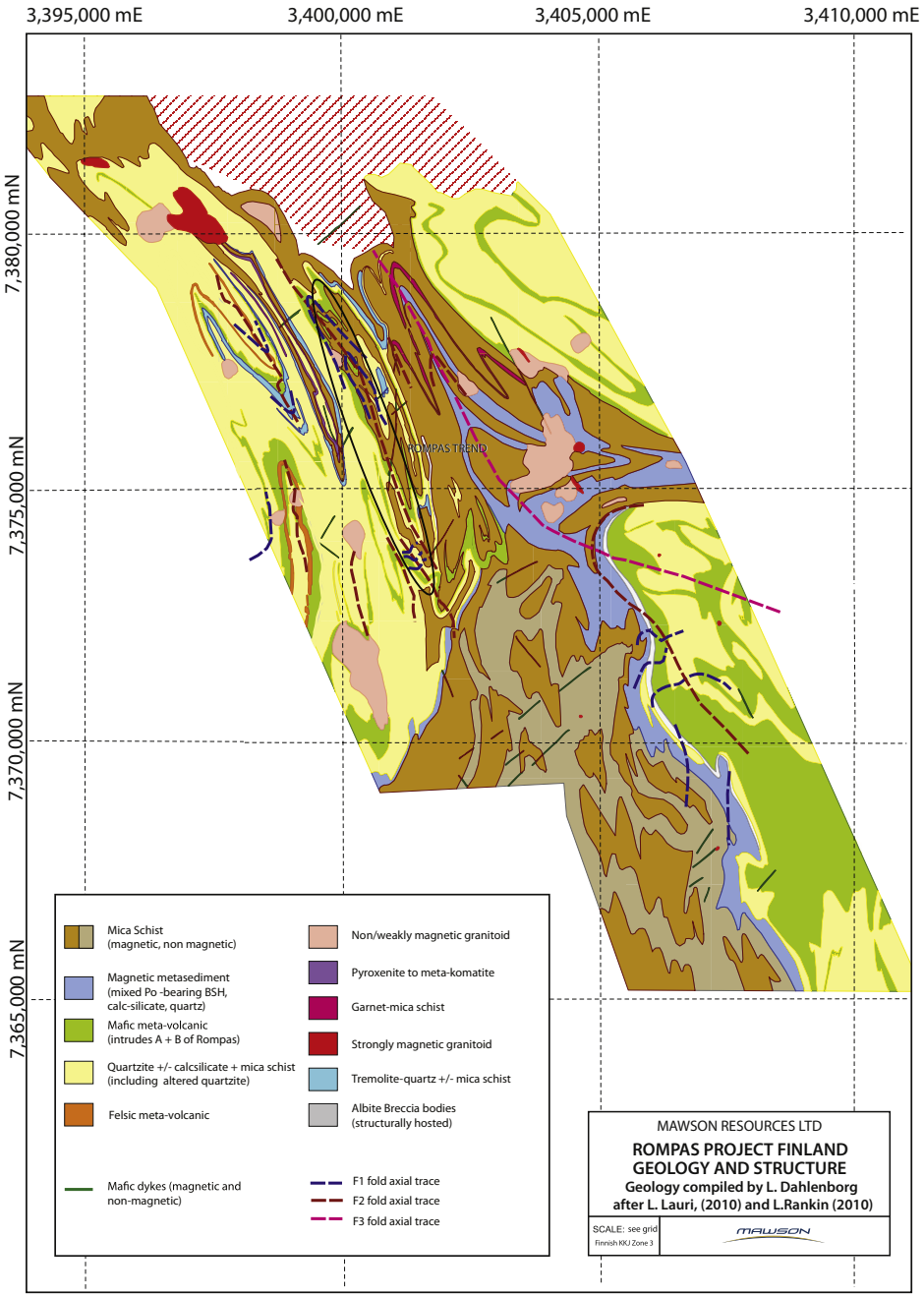


**FIGURE 5.4.3 Geological map centered on Rompas prospect based on outcrop observations and interpretation of aeromagnetic images.**

The Rompas trend is shown within the black ellipse.

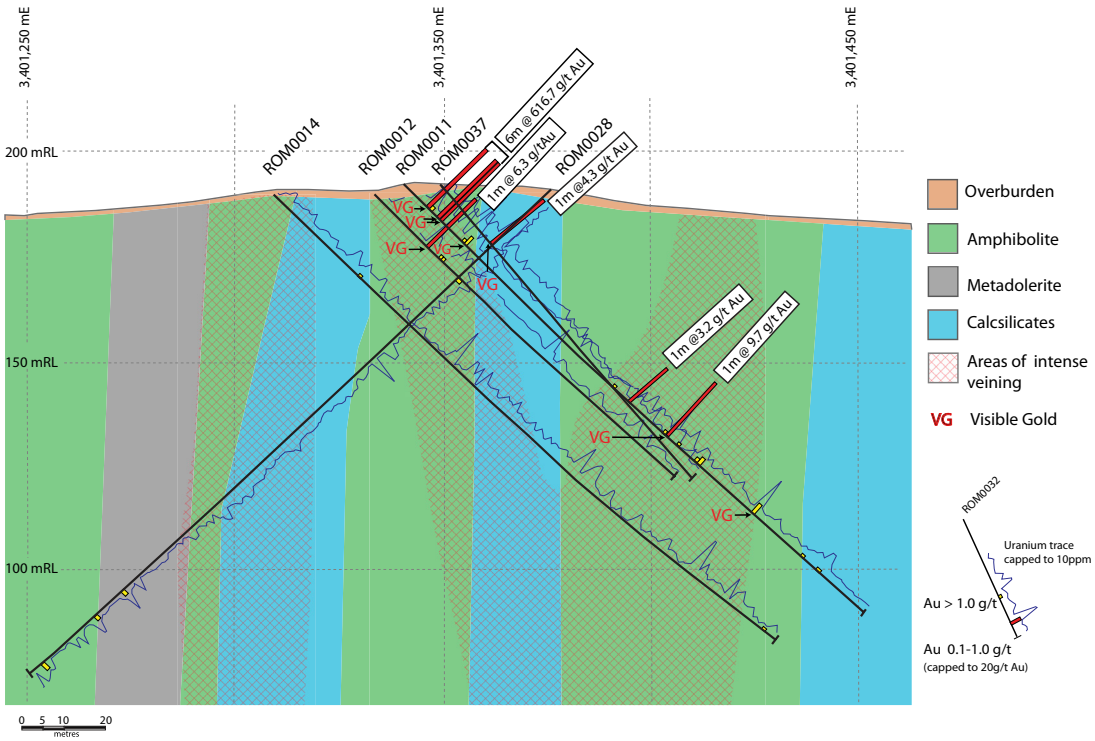


**FIGURE 5.4.4 Cross section from South Rompas passing through ROM0011.**

Note the metabasalt units within the calc-silicate (+ albite) rocks and metadolerite in the western part of the section. Gold intersections and the uranium traces are placed on the drill holes. The red hatched area indicates the most intense mineralization, but note that the high gold values are only within the mafic rocks.

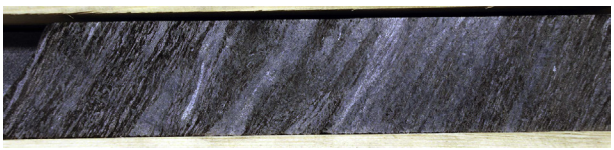

**FIGURE 5.4.5 Metabasalt with strong foliation defined by biotite-amphibole-rich zones (dark) and lighter albitic alteration bands at South Rompas.**

Some of the light bands appear to be marginal to highly attenuated dolomite–calc-silicate veins. The drill core is 48 mm wide.

Using the $TiO_2$ content (Table 5.4.1) as an indicator of mafic precursor has proved successful to gain confidence in visual logging of the drill core.

Within the metabasalts, variably oriented larger amphibole grains up to 8 mm long grow across the S2 foliation throughout the North and South Rompas prospect areas. The amphibole compositions may vary from cummingtonite to anthophyllite, in addition to pargasitic hornblende. Indeed, individual samples may

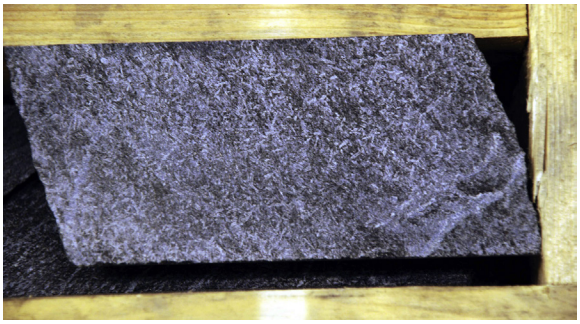

**FIGURE 5.4.6 Mafic rock preserving a doleritic igneous texture at North Rompas.**

The former euhedral feldspars are recrystallized and lie within a matrix of amphibole and biotite. The drill core is 48 mm wide.

contain three amphiboles, namely hornblende, cummingtonite, and anthophyllite. Fine-grained pyrrhotite is the dominant sulfide away from mineralized veins, with rarer chalcopyrite and scarce pentlandite. Magnetite is largely absent from South Rompas, but is widespread in the mafic rocks at North Rompas. Rare fine graphite lies within the foliation planes adjacent to the mineralization at ROM0011, although the distribution of graphite in the mafic rocks has not been carefully checked in other locations. Assemblages in the main foliation in the metabasalts are compatible with amphibolite facies metamorphism.

Within both the mafic units and the calc-silicate-albite rocks are common metamorphosed dolomite ± quartz veins, now comprising largely dolomite, calcite, diopside, quartz, and actinolite. These veins are the hosts to the uraninite-gold mineralization, but only where they occur within metabasalt. Of particular importance, however, is the observation that these calc-silicate-carbonate-quartz veins are as abundant in the enclosing metasediments (Fig. 5.4.7) as they are within the mafic rocks. Alteration on the margins of both mineralized and unmineralized veins, such as in ROM0034, is typically biotite and albite rich, totally destroying the primary igneous textures in the metabasalt.

The western boundary of the Au-U occurrence in mafic rocks is marked by a thin, highly conductive graphitic unit of siltstone or mudstone protolith. This lies within a sequence of interbedded aluminous-biotite schists and arkosic to moderately quartzose metamorphosed siltstones and sandstones. Interspersed with these clastic metasediments are mafic units and carbonate rocks. Mineral assemblages in the aluminous schists include muscovite-biotite-feldspar-quartz ± garnet (South Rompas; Fig. 5.4.8) to sillimanite, cordierite, and garnet-bearing metapelites (Fig. 5.4.9) adjacent to the North Rompas occurrence. Metamorphic grade is therefore proposed to increase over the 6 km from South Rompas to conditions above the muscovite stability field at North Rompas.

Three significant deformational events are recognized at Rompas, although these are yet to be correlated with fold generations in the less metamorphosed, southern portions of the PSB. North, Central, and South Rompas lie on a largely linear trend (see Fig. 5.4.3), generated by the interaction of folds inferred to be related to D2 and D3 deformational events. The D1 event in the Rompas area is difficult to identify, but regional work (e.g., Terry Lees and Leigh Rankin, unpublished reports to Mawson Resources) suggests it is now present as transposed isoclinal folds with the foliation defined by amphibolite facies assemblages parallel or subparallel to the D2 foliation. D2 formed upright N-striking tight to isoclinal folds. Of significance at Rompas is that the D2 foliation is quite variable in intensity, with an increase toward South

**Table 5.4.1 A representative selection of whole-rock analyses from the Rompas prospect, including mineralized and calc-silicate veined mafic rocks (mb) and the enclosing calc-silicate (Cs) rocks**

| Hole ID | ROM0011 | ROM0011 | ROM0011 | ROM0011 | ROM0014 | ROM0014 | ROM0014 | ROM0014 | ROM0028 | ROM0028 |
|---|---|---|---|---|---|---|---|---|---|---|
| Sample ID | 226218 | 226219 | 226241 | 226297 | 226484 | 226547 | 226552 | 226642 | 229315 | 229446 |
| Depth from (1 m samples) | 11 | 12 | 33 | 87 | 7 | 67 | 71 | 159 | 16 | 141 |
| Rock type | mb | mb | cs | mb | cs | mb | cs | mb | cs | mb |
| $SiO_2$[a] | 54 | 51 | 62 | 54 | 59 | 52 | 58 | 56 | 61 | 50 |
| $TiO_2$ | 1.62 | 1.10 | 0.67 | 1.51 | 0.46 | 2.12 | 0.44 | 1.21 | 0.63 | 1.50 |
| $Al_2O_3$ | 12.96 | 9.09 | 14.21 | 11.62 | 11.07 | 14.15 | 11.49 | 11.70 | 14.28 | 12.13 |
| FeO | 10.97 | 7.89 | 5.18 | 9.73 | 5.80 | 14.60 | 2.42 | 2.83 | 3.49 | 11.03 |
| MnO | 0.10 | 0.14 | 0.02 | 0.07 | 0.06 | 0.09 | 0.05 | 0.04 | 0.03 | 0.16 |
| MgO | 5.41 | 9.45 | 2.67 | 7.31 | 7.45 | 6.92 | 6.88 | 7.46 | 3.33 | 8.64 |
| CaO | 5.96 | 15.18 | 4.70 | 8.00 | 8.54 | 3.79 | 12.06 | 12.30 | 7.39 | 11.18 |
| $Na_2O$ | 2.76 | 2.16 | 6.98 | 3.24 | 4.19 | 3.59 | 6.17 | 5.93 | 7.98 | 2.39 |
| $K_2O$ | 3.43 | 1.66 | 0.89 | 1.45 | 1.24 | 0.31 | 0.39 | 0.17 | 0.19 | 0.98 |
| $P_2O_5$ | 0.22 | 0.14 | 0.13 | 0.18 | 0.10 | 0.26 | 0.11 | 0.20 | 0.13 | 0.18 |
| S | 0.30 | 0.01 | 0.02 | 0.05 | 0.01 | 0.19 | 0.00 | 0.00 | 0.00 | 0.07 |
| Au | 3540 | 137 | <0.001 | 9.58 | 0.013 | 0.007 | 0.003 | 0.001 | 0.01 | 0.35 |
| Pb | 780 | 252 | 4.5 | 117.5 | 4.3 | 3 | 4.9 | 3.7 | 3.9 | 7.6 |
| U | 1770 | 650 | 2.3 | 338 | 2.6 | 0.7 | 3.2 | 2.1 | 2.5 | 6 |
| Ag | 12.55 | 0.84 | 0.03 | 0.35 | 0.04 | 0.08 | 0.02 | 0.05 | 0.05 | 0.11 |
| As | 79.4 | 35 | <0.2 | 1.2 | <0.2 | <0.2 | <0.2 | 0.3 | 0.5 | 1.5 |
| Be | 1.04 | 0.7 | 0.96 | 0.78 | 0.78 | 0.55 | 0.8 | 0.48 | 0.66 | 0.7 |
| Bi | 22.4 | 0.66 | 0.01 | 0.06 | 0.08 | 0.02 | 0.02 | 0.03 | 0.01 | 0.22 |
| Ce | 47 | 50 | 55.4 | 34.5 | 49.3 | 52.2 | 50.1 | 30.7 | 60.8 | 52.9 |
| Co | 54.3 | 39 | 3.7 | 43.5 | 20.2 | 62.5 | 3.1 | 6.4 | 2.1 | 62.4 |
| Cs | 6.26 | 2.22 | 1.17 | 2.28 | 1.31 | 0.42 | 0.15 | 0.07 | 0.18 | 1.29 |
| Cu | 120 | 4.6 | 1.6 | 64.3 | 1.8 | 138.5 | 3.3 | 4.1 | 1.2 | 59.6 |
| Ga | 22.6 | 15.05 | 19.1 | 19.75 | 16.55 | 22.7 | 18.6 | 16.5 | 22.9 | 19.85 |
| Ge | 0.24 | 0.18 | 0.13 | 0.26 | 0.14 | 0.25 | 0.14 | 0.13 | 0.19 | 0.15 |
| Hf | 4.9 | 3.4 | 4.8 | 3.9 | 3.4 | 6 | 3.5 | 3.6 | 3.8 | 4.5 |

| | | | | | | | | | | |
|---|---|---|---|---|---|---|---|---|---|---|
| In | 0.082 | 0.065 | 0.006 | 0.055 | 0.056 | 0.106 | 0.007 | 0.012 | <0.005 | 0.102 |
| La | 21.4 | 23.8 | 29.3 | 16.6 | 24.8 | 24.2 | 26 | 15.5 | 31 | 27.1 |
| Mo | 15.4 | 25.2 | 0.13 | 3.15 | 0.51 | 1.51 | 0.15 | 0.57 | 0.14 | 3.44 |
| Nb | 8.4 | 5.3 | 7.9 | 6.7 | 6.1 | 9.6 | 5.1 | 5 | 7.8 | 7.3 |
| Ni | 195.5 | 117.5 | 43.7 | 68.1 | 63.8 | 57.3 | 38.4 | 23.9 | 27.2 | 82.1 |
| Rb | 104 | 44.2 | 26.2 | 45.4 | 31.8 | 7.6 | 7.1 | 2.8 | 4.5 | 27.2 |
| Re | 0.042 | 0.036 | <0.002 | 0.004 | <0.002 | 0.003 | <0.002 | <0.002 | <0.002 | 0.004 |
| Sb | 4.38 | 0.83 | 0.27 | 0.21 | 0.12 | 0.1 | 0.26 | 0.35 | 0.42 | 0.19 |
| Sn | 1.4 | 1.2 | 1.9 | 0.7 | 1.4 | 1.9 | 1.1 | 2.1 | 1.9 | 1.1 |
| Ta | 0.46 | 0.31 | 0.67 | 0.4 | 0.53 | 0.6 | 0.43 | 0.31 | 0.62 | 0.44 |
| Te | 103 | 11.45 | <0.05 | 0.17 | 0.06 | 0.05 | <0.05 | <0.05 | c0.05 | 0.25 |
| Th | 14.9 | 4.2 | 11.3 | 5.9 | 7.9 | 4.9 | 8.6 | 5.3 | 10.5 | 3.6 |
| Tl | 0.48 | 0.17 | 0.06 | 0.15 | 0.1 | 0.03 | 0.03 | <0.02 | <0.02 | 0.07 |
| V | 300 | 300 | 113 | 284 | 107 | 286 | 94 | 179 | 124 | 254 |
| W | 4.4 | 2.1 | 1.1 | 2.3 | 1 | 0.7 | 3.9 | 16.1 | 5 | 0.8 |
| Y | 34.8 | 37.6 | 16.4 | 24.6 | 18.9 | 28.2 | 18.4 | 20.2 | 15.4 | 39.8 |
| Zn | 89 | 79 | 8 | 28 | 21 | 24 | 17 | 8 | 7 | 30 |
| Zr | 175.5 | 123.5 | 162 | 146.5 | 122 | 213 | 123.5 | 129.5 | 151.5 | 154 |
| Sr (%) | 0.005 | 0.010 | 0.004 | 0.005 | 0.004 | 0.003 | 0.004 | 0.005 | 0.005 | 0.013 |
| Cr (%) | 0.011 | 0.008 | 0.016 | 0.008 | 0.012 | 0.009 | 0.010 | 0.006 | 0.011 | 0.009 |
| Ba (%) | 0.020 | 0.012 | 0.008 | 0.004 | 0.010 | 0.003 | 0.003 | 0.001 | 0.002 | 0.008 |
| Albite (%) | 23.38 | 18.25 | 59.08 | 27.37 | 35.47 | 30.34 | 52.24 | 50.19 | 67.52 | 20.19 |

*Note: Refer to Fig. 5.4.3 for the location of the samples. The analyses were conducted by Australian Laboratory Services (ALS) using ICP-MS, excluding gold, which was analyzed using fire assay techniques. Negative numbers refer to the detection limits of the individual elements. All trace elements with the exception of Sr, Cr, and Ba are reported in parts per million.*

*[a]$SiO_2$ is estimated by difference as the acid digest and ICP method prevented analysis. Albite percentage has been estimated on the assumption of all $Na_2O$ is contained within albite.*

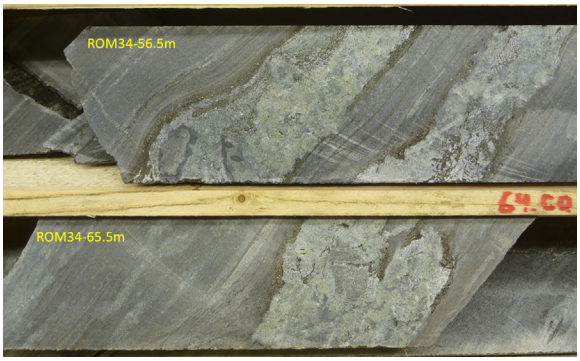


**FIGURE 5.4.7 Albite-altered metasediments with dolomite-diopside-actinolite-quartz-calcite veins.**

Note the biotite-rich selvages on the veins. Note that these metasediments enclosing the mineralized Rompas mafic rocks lack any peraluminous minerals other than biotite and typically contain some fine-grained calc-silicate minerals (ROM0034 drill hole, core diameter is 48 mm).

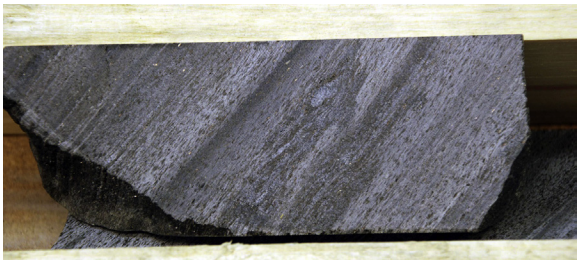

**FIGURE 5.4.8 Possible graded bedding within biotite-muscovite metapelites from South Rompas.**

These rocks are characteristic of the metasediments from basin stage 3. Drill core is 48 mm across.

**FIGURE 5.4.9 Garnet porphyroblasts in sillimanite-biotite gneiss from North Rompas.**

Diamond saw cut across outcrop was for sampling purposes. Scribe is 150 mm long.

Rompas to such an extent that any protolith textures are destroyed. Relatively low-strain rocks are described at North Rompas, preserving vesicles and pillow structures in mafic rocks, whereas at South Rompas, in particular, total strain is very high and relic early structures are difficult to identify.

Transposition of lithologic contacts in the amphibolite facies rocks is observed at both outcrop and regional scales (from interpretation of aeromagnetic data). Superimposed on the D2 foliation at South Rompas is significant extension-producing boudinage of veins (Fig. 5.4.10) and subvertically plunging, cigar-shaped dolomite pods. These dolomite pods are important as they are a common host to large porphyroblastic uraninite and extreme gold values, with some samples at South Rompas exceeding 10,000 g/t Au! Unfortunately, the linear nature and the lack of predictability in location of these pods within the mafic rocks makes for a difficult drill target. Weathering of the carbonate in these pods produces deep brown soils with abundant residual gold that is recoverable with panning (Fig. 5.4.11).

**FIGURE 5.4.10 Examples of boudinaged veins from the Rompas trend.**

*Top:* South Rompas drilling area (field of view 50 cm). *Bottom:* Western end of "The Wall" at North Rompas (field of view 1 m). Cavities within the vein are dolomite and calcite with uraninite.

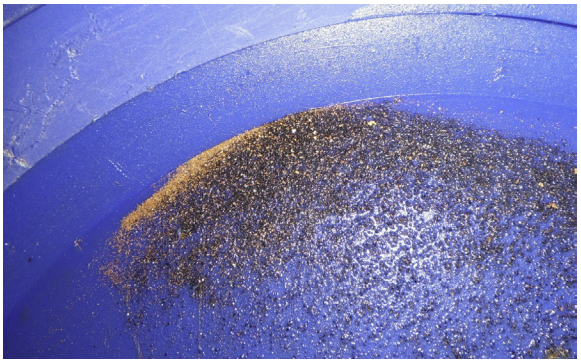

**FIGURE 5.4.11 The results of gold panning above a subvertical weathered dolomitic pod.**

These are clearly evident in this photo. Approximately 1 kg of sample was panned. Field of view is 10 cm.

At least one brittle, post-metamorphic deformation episode is proposed. Late fractures filled with calcite and quartz are common, and some may be synchronous with the last stages of gold mineralization and brittle fracturing of uraninite. In one location, a concretion-like mass of pyrobitumen is enclosed in a calcite-filled fracture, compatible with the observations on mineralization detailed in the following.

Understanding the geochemistry of the host mafic sequence to the mineralization is complicated by variable alkali, Mg, and S mobility and dilution of less mobile components. A selection of representative analyses of the mafic host rocks and albite–calc-silicate metasediments is presented in Table 5.4.1 (note that $SiO_2$ in these analyses is unreliable as it is not determined by the inductively coupled plasma mass spectrometry (ICP-MS) method but has been calculated here by difference and should be regarded as an approximation only). Many 1-m intervals contain significant dolomite–calc-silicate–quartz veining and some data trends are a function of dilution by dolomite, rather than an inherent original chemical variation in the mafic precursor. This is evident, for example, in the data from ROM0011—the 1-m interval commencing at 12 m (down-hole depth) is diluted approximately 40% by veining. The corresponding decrease in $TiO_2$ is a function of this dilution, rather than protolith variation. Rare earth element (REE) studies of Rompas mafic rocks are confined to Mustonen (2012), who regarded the REE profiles to most closely match that of the Runkaus basalts, the lowermost mafic volcanics of the Peräpohja Belt. This interpretation is, however, questioned by us, as the Rompas host rocks appear to be at a higher stratigraphic position than the Runkaus formation rocks (Fig. 5.4.2).

## MINERALIZATION

In terms of exploration for gold and uranium, distribution within the initial discovery area at Rompas is best described as nuggety. The discovery of gold at the surface is directly associated with the ability to find uraninite using a scintillometer or spectrometer, and a till cover of more than 1 m will generally reduce the radioactivity to background levels. Visible gold largely occurs within uraninite, with the coarsest grains occurring within and associated with the dolomite pods described previously (Fig. 5.4.12; South Rompas). Gold occurs as fracture-controlled veinlets, in places extending beyond the uraninite and onto cleavage surfaces on carbonate, and more rarely on quartz. At North Rompas, visible gold is

**FIGURE 5.4.12 A small vein of gold within dolomite and fine dark amphibole.**

Note the finely disseminated gold throughout the sample as the likely "hard rock" source of the gold recovered by panning in the in the soils above occurrences of weathered carbonate rocks (South Rompas). The sample is 1.5 cm long.

also present as equigranular aggregates within actinolite, spatially associated with porphyroblastic uraninite grains (Fig. 5.4.13). Visible gold surrounding pyrobitumen with associated molybdenite has been observed in ROM0084, drilled immediately below the spectacular gold intersection in ROM0011 (Fig. 5.4.14). Porphyroblastic uraninite typically has a distinctive pink to reddish albite alteration halo extending from the carbonate–calc-silicate veins into albitic margins (Fig. 5.4.15).

No geophysical responses have been detected to the mineralization. Fine pyrrhotite is a ubiquitous trace component of the metabasalt, resulting in a stronger IP chargeability response than the adjacent rocks, but the intensity of response is not directly associated with gold. It is useful, however, for mapping the occurrence of metabasalt under the till.

Thin and very high-grade drill intercepts are common, such as for the sample 11–12 m down-hole depth shown in Table 5.4.1 and Fig. 5.4.14, matching the many hundred surface trench

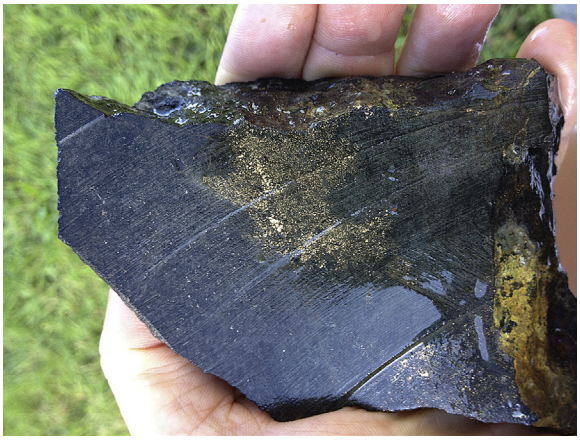

**FIGURE 5.4.13 Spectacular gold within actinolite.**

Actinolite is dominant across all except the lower right corner, where a dark, large uraninite grain occurs. The uraninite is difficult to see in the photo, but is responsible for the secondary yellow uranium products on the extreme lower right fractured surface. Thin-section examination shows a polygonal equigranular intergrowth of gold and actinolite indicating coeval formation or recrystallization. The sample is from the North Rompas diamond sawn trench at surface and is 10 cm in its longest dimension.

**FIGURE 5.4.14 Dolomite–calc-silicate vein with bonanza gold grades from ROM0011.**

The grade for this 1 m at 11–12 m down-hole depth is 3540 g/t, part of the 6 m at 617 g/t intersection. The drill core is 63 mm across.

**FIGURE 5.4.15 Uraninite grain 15 mm across within a dolomite–calc-silicate vein with thin biotite selvage enveloped by albite-rich alteration of metabasalt.**

Note the reddish albite, a common feature adjacent to uraninite.

exposures of bonanza grades found over the 6 km trend. Full details of intersections are reported on the Mawson Resources website (www.mawsonresources.com). What is clear from the drilling and trenching at North and South Rompas is the strong host rock control on mineralization—the metabasalt. Uraninite and gold are found within or marginal to carbonate–calc-silicate–quartz veins in the metabasalt. Vein densities in the adjacent metasedimentary albitic calc-silicate rocks are similar to the metabasalt, but to date lack any significant Au or U. Thus, interaction with some component in the basalt is inferred to be the key control on uraninite precipitation, with a secondary mechanism favored to precipitate gold at a later stage.

On the basis of bulk rock analyses, the gold itself is of high fineness, recording more than 95% Au, with minor Ag and Cu. Drilling up to 100 m vertical depth has not revealed any variation in the fineness. Petrographic examination by prior workers reveals that the gold is paragenetically later than the uraninite, commonly occupying cracks within uraninite (Figs. 5.4.16 and 5.4.17; plus descriptions by Gaillard, 2012; and Ashley, internal company reporting). Some secondary U-Th minerals such as coffinite and thorite are also present. Paragenetically late gummite is locally present in surface samples occurring between uraninite grains (Gaillard, 2012). In most outcrops where uraninite has been recorded, secondary yellow uranium minerals have been observed on fractures and surface coatings.

As noted before, gold occurs in two modes, the first within fractures in uraninite within the calc-silicate veins, and the second generally as crusts on the spherical to subrounded undeformed pyrobitumen. Pyrobitumen also occurs as rims and nodular accretions around uraninite in textures reminiscent of radiolytic polymerization.

The uraninite within the pyrobitumen nodules contains more than five times the $ThO_2$ and $Y_2O_3$ contents of the coarse-grained uraninites in the dolomite–calc-silicate veins and the Pb contents are a function of the alteration content. Preliminary U-Th-Pb age determinations show a clustering of ages of the least altered uraninite grains reflecting the peak of metamorphism of the host sequence, but we are uncertain of the significance of this in terms of the regional tectonic history of the Fennoscandian Shield.

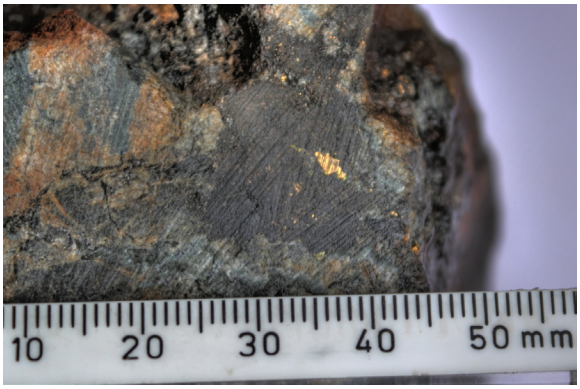


**FIGURE 5.4.16 A large (15 mm) uraninite grain within dolomite–calc-silicate vein.**

Note gold within diagonally trending fracture across the uraninite and disseminated gold toward top of photo.

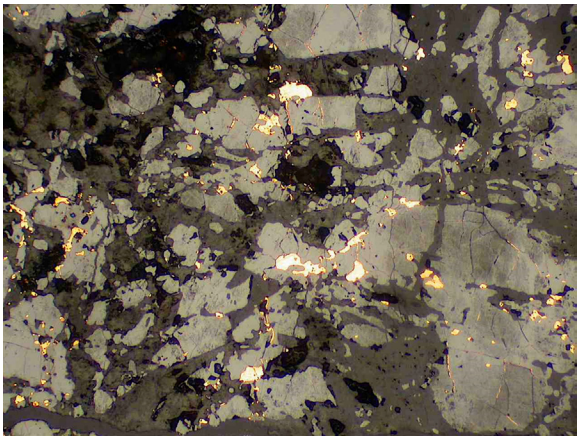

**FIGURE 5.4.17 Reflected light photomicrograph of intensely fractured uraninite (light gray) with gold filling fracture networks.**

Some larger "blobs" of gold on the outside of uraninite grains are with carbonate and silicate matrix (dark gray). Note the variable reflectivity of the uraninite—there are both strongly reflective, "clean" uraninite grains and many with a cloudy appearance. These have different trace element and Pb concentrations. Field of view is 5 mm.

The gold within the coarse porphyroblastic uraninite is associated with galena, altaite, nickeline, cobaltite, and rare Pb-bearing maldonite, hunchunite, and auricupride. In contrast, the gold associated with pyrobitumen is more closely related to a pyrite, pyrrhotite, chalcopyrite, galena, altaite, molybdenite, Bi-telluride, and titanite assemblage (Figs. 5.4.18, 5.4.19, and 5.4.20). Reflectance measurements conducted on the undeformed pyrobitumen nodules containing gold indicates a likely maximum maturation temperature of between 270° and 340 °C, which is probably reflecting the formation temperature of the gold mineralization. The Pb-bearing minerals (e.g. galena, altaite), associated with

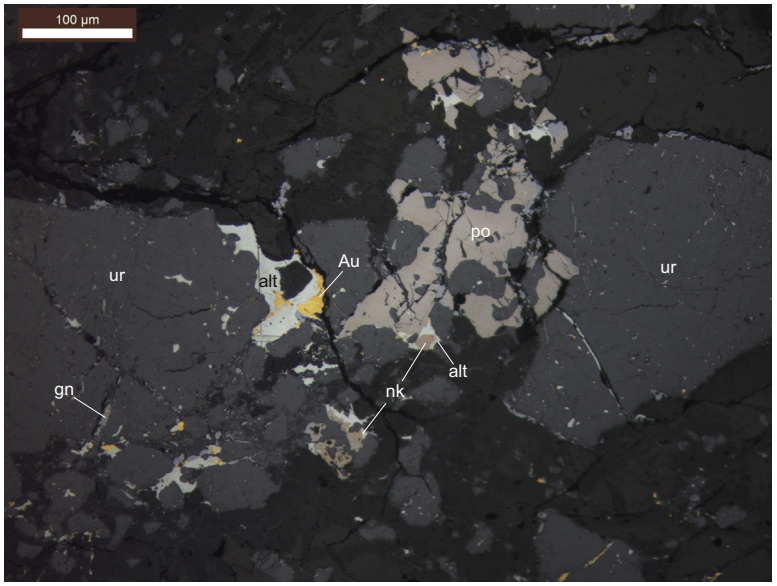


**FIGURE 5.4.18 Large mid-gray uraninite (Ur) grains with very fine galena (Gn) throughout.**

The more reflective light-bluish-white grains are altaite (alt), which is host to gold in the center part of the picture. Pyrrhotite (po) is the light brown mass in the center and upper part of the image. A small grain of nickeline hosted by altaite is attached to the pyrrhotite in the center of the picture. The groundmass hosting the crushed uraninite grains is carbonate. Field of view is 0.65 mm.

Source: *Photo by F. Molnár.*

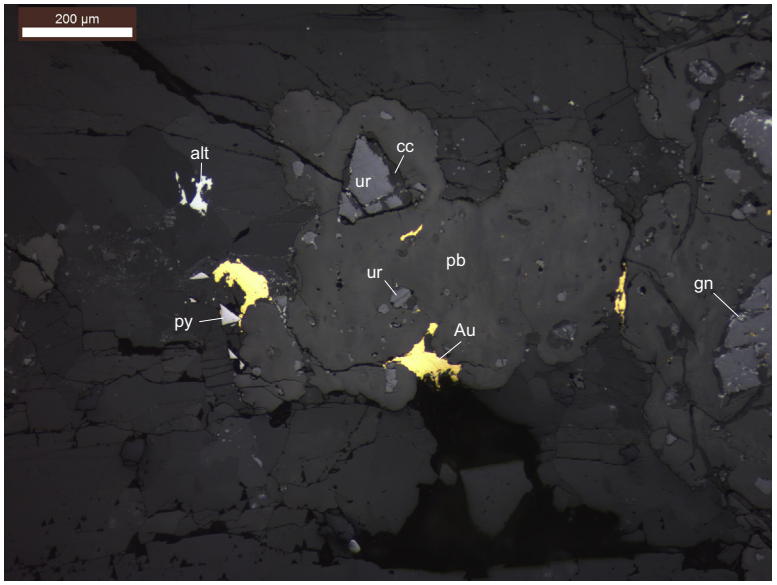


**FIGURE 5.4.19 Nodular "blobs" of pyrobitumen within a matrix of carbonate (dark gray).**

The medium gray fragments throughout the pyrobitumen are uraninite, including the larger, triangular fragment in the upper center of photo. The dark gray crust on some of the uraninite grains (e.g. the triangular one in the upper center) is carbonate. The very bright white grain with triangular shape next to the gold at left-center is pyrite. The bright fields above this gold grain are altaite (alt) grains (in calcite). Field of view is 1.25 mm.

Source: *Photo by F. Molnár.*

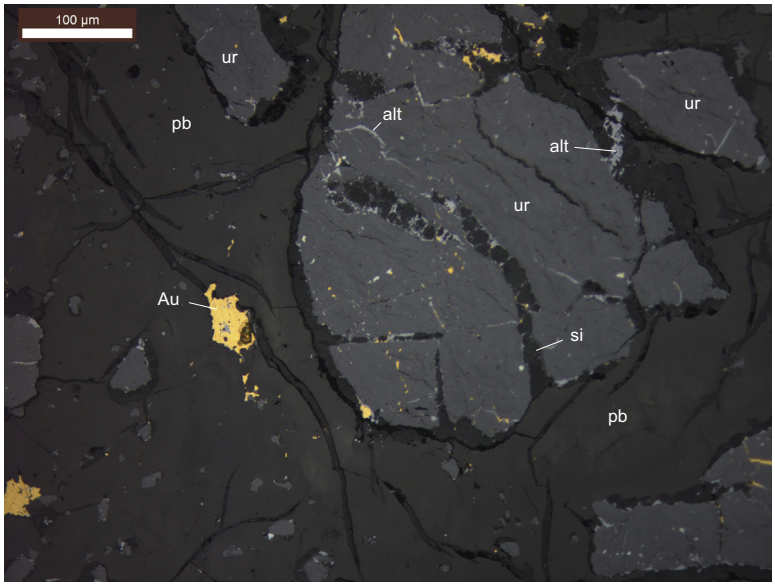


**FIGURE 5.4.20 Amorphous silica (Si) filling cracks in uraninite grains enclosed within slightly desiccated pyrobitumen.**

The bluish white phase in fractures is altaite (alt). Note the gold within microfractures in uraninite and associated with the pyrobitumen and amorphous silica. Field of view is 0.65 mm.

Source: *Photo by F. Molnár.*

the first stage of gold formation, are highly radiogenic. We infer that a sulfur-bearing fluid carrying gold has precipitated the Pb minerals, scavenging radiogenic lead from the uraninite. In addition, early indications of the age of molybdenite associated with pyrobitumen (H. Stein, personal communication) indicate an age close to 1.78 Ga, representing some 150-million-year difference between the formation of the uraninite and the gold-pyrobitumen (+ molybdenite). These later dates are compatible with the ages of the Central Lapland Granite Complex, concentrated around the 1.81 to 1.78 Ga range (e.g., Lauri, 2012).

## SUMMARY

We consider it most likely that the uraninite with the dolomite–calc-silicate veins at Rompas was metamorphosed to amphibolite facies conditions and deformed approximately 1.95 Ga ago. This matches unpublished data of Cathelineau et al. (CREGU internal report to Mawson Resources, and in prep.). The "pre-metamorphic" age of the uraninite remains uncertain, but is evidently older than 1.95 Ga. Critically, a much younger age of approximately 1.78 Ga is proposed by us as the age of the gold mineralization, based on the textural, geochemical, and preliminary isotopic data. At least two gold-bearing sulfurous fluids, the first reacting with radiogenic lead from uraninite, and a second, lower temperature fluid, reacted with pyrobitumen, resulted in gold formation with close spatial relationships to uraninite. Further exploratory drilling and laboratory studies will no doubt provide more detailed and more robust insights into the formation of the Rompas uranium-gold occurrences.

## ACKNOWLEDGMENTS

Very few mineral occurrences are found by the efforts of one person alone, and Rompas is no exception. The combination of regional geologic evaluation, through district-scale research to detailed ground checking, is acknowledged here. The Mawson exploration team presently comprises six geologists directly working on the project (Erkki Vanhanen, Nick Cook, Mike Hudson, Tuomas Havela, Janne Kinnunen, and Lars Dahlenborg). Former staff on the project, consultants, and summer students have added significantly to the understanding of the Rompas-Rajapalot project and include, but are not limited to, Jukka-Pekka Ranta, Terry Lees, Jan-Anders Perdahl, Claude Caillat, Leigh Rankin, Gerald Purvis, Nicolas Gaillard, Pertti Sarala, Eelis Pulkkinen, David McInnes, Hans Thunehed, and Marcus Tomkinson. In addition, research groups based at the GTK (Ferenc Molnár, Esa Pohjolainen, Antonin Richard, Laura Lauri) and at Nancy/CEGRU/AREVA (Michel Cathelineau, Marc Brouand) have been instrumental in allowing Mawson to further develop an understanding of the mineralization at Rompas.

## REFERENCES

Eilu, P., Pankka, H., Keinänen, V., Kortelainen, V., et al., 2007. Characteristics of gold mineralisation in the greenstone belts of northern Finland. Geological Survey of Finland, Special Paper 44, 57–106.

Gaillard, N., 2012. Les concentrations en or et uranium dans les niveaux de calc-silicates du nord de la Finlande (Rovaniemi). M.Sc. thesis. Universite Henri Poincare (Nancy), p. 42.

Halkoaho, T., Iljina, M., 2012. Portimo Cr, PGE-Ni. Geological Survey of Finland Special Paper 53, 294–298.

Hanski, E., Huhma, H., Perttunen, V., 2005. SIMS U-Pb, Sm-Nd isotope and geochemical study of an arkosite-amphibolite suite, Peräpohja schist belt: evidence for ca. 1.98 Ga A-type volcanism in northern Finland. Bulletin of the Geological Society of Finland 77, 5–29.

Huhma, H., Cliff, R., Perttunen, V., Sakko, M., 1990. Sm-Nd and Pb isotopic study of mafic rocks associated with early Proterozoic continental rifting: the Peräpojha schist belt in northern Finland. Contributions to Mineralogy and Petrology 104, 367–379.

Huhma, H., O'Brien, H., Lahaye, Y., Mänttäri, 2011. Isotope geology and Fennoscandian lithosphere evolution. In: Nanonen, K., Nurmi, P.A. (Eds.), Geological Survey of Finland, Special Paper, 49, pp. 35–48.

Karhu, J., 1993. Paleoproterozoic evolution of the carbon isotope ratios of sedimentary carbonates in the Fen noscandian Shield. Geological Survey of Finland, Bulletin 371, 87.

Kyläkoski, M., Eilu, P., Perdahl, J.-A., 2012a. Peräpohja Cu-Co. Geological Survey of Finland Special Paper 53, 301–302.

Kyläkoski, M., Hanski, E., Huhma, H., 2012b. The Petäjäskoski formation, a new lithostratigraphic unit in the Paleoproterozoic Peräpohja belt, northern Finland. Bulletin of the Geological Society of Finland 84, 85–120.

Lauri, L., 2012. Temporal and Hf isotopic geochemical evolution of southern Finnish Lapland from 2.77 Ga to 1.76 Ga. Bulletin of the Geological Society of Finland 84, 121–140.

Mustonen, M., 2012. Geochemistry and petrography of the volcanic rocks in the Rompas area, Ylitornio, northern Finland. M.Sc. thesis, University of Oulu, p. 63.

Niiranen, T., 2012. Misi Fe. Geological Survey of Finland Special Paper 53, 304–306.

Niiranen, T., Hanski, E., Eilu, P., 2003. General geology, alteration, and iron deposits in the Palaeoproterozoic Misi region, northern Finland. Bulletin of the Geological Society of Finland 75, 69–92.

Perttunen, V., Hanski, E., 2003. Koivu and Törmäsjärvi. Explanation to the Geological Map of Finland 1 100 000, pre-Quaternary rocks, sheets 3631 and 2633. Geological Survey of Finland, p. 88. (in Finnish, with English summary).

Perttunen, V., Hanski, E., Väänänen, J., et al., 1996. Rovaniemin kartta-alueen Kallioperä. Geological Map of Finland 1 100 000. Explanation to the maps of pre-Quaternary rocks, sheet 3612.

Ranta, J.-P., 2012. Peräpohjan liuskealueen pohjoisosan yksiköiden zirkoniajoitus U-Pb-menetelmällä. M.Sc. thesis. Department of Geosciences. University of Oulu, p. 89 (in Finnish).